J Mol Model (2008) 14:987–994
DOI 10.1007/s00894-008-0348-2

ORIGINAL PAPER

The anti-fibrillogenic activity of tetracyclines on PrP 106–126: a 3D-QSAR study

Ugo Cosentino · Demetrio Pitea · Giorgio Moro · Gloria A. A. Saracino · Pietro Caria · Rosaria M. Varì · Laura Colombo · Gianluigi Forloni · Fabrizio Tagliavini · Mario Salmona

Received: 19 February 2008 / Accepted: 24 June 2008 / Published online: 16 July 2008

Abstract There is evidence that Tetracyclines are potentially useful drugs to treat prion disease, the fatal neurodegenerative disease in which cellular prion proteins change in conformation to become a disease-specific species (PrP^{Sc}). Based on an *in vitro* anti-fibrillogenesis test, and using the peptide PrP106–126 in the presence of tetracycline and 14 derivatives, we carried out a three-dimensional quantitative structure-activity relationship (3D-QSAR) study to investigate the stereoelectronic features required for anti-fibrillogenic activity. A preliminary variable reduction technique was used to search for grid points where statistical indexes of interaction potential distributions present local maximum (or minimum) values. Variable selection genetic algorithms were then used to search for the best 3D-QSAR models. A 6-variable model showed the best predictability of the anti-fibrillogenic activity that highlighted the best tetracycline substitution patterns: hydroxyl group presence in positions 5 and 6, electrodonor substituents on the aromatic D-ring, alkylamine substituent at the amidic group in position 2 and *non-epi* configuration of the NMe_2 group.

Keywords Anti-amyloidogenic activity · Prion protein · Tetracycline derivatives · 3D-QSAR analysis

U. Cosentino (✉) · D. Pitea · P. Caria
Dipartimento di Scienze dell'Ambiente e del Territorio,
Università degli Studi di Milano-Bicocca,
Milan, Italy
e-mail: ugo.cosentino@unimib.it

G. Moro · G. A. A. Saracino
Dipartimento di Biotecnologie e Bioscienze,
Università degli Studi di Milano-Bicocca,
Milan, Italy

R. M. Varì
Dipartimento del Farmaco, Istituto Superiore di Sanità,
Rome, Italy

L. Colombo · G. Forloni · M. Salmona
Istituto di Ricerche Farmacologiche "Mario Negri",
Milan, Italy

F. Tagliavini
Fondazione IRCCS "Carlo Besta",
Milan, Italy

Introduction

Transmissible spongiform encephalopathies (TSEs), or prion disease, [1] are a group of neurodegenerative disorders that can have sporadic, infectious or genetic origins, including scrapie and bovine spongiform encephalopathy in animals, and Creutzfeldt-Jakob disease (CJD), Gerstmann-Sträussler-Scheinker disease (GSS), and fatal familial insomnia (FFI) in humans. The basis of the pathogenic mechanism is a conformational modification of the cellular prion protein (PrP^{C}), resulting in a protease resistant isoform termed PrP^{Sc}. Indeed, PrP^{Sc} is responsible for neuronal degeneration and glial activation, [2] and is critical for disease transmissibility as it converts PrP^{C} to the PrP^{Sc} isoform. [3, 4]

Different classes of compounds, including Amphotericin B, branched polyamines, Congo Red, Iododoxorubicin, Quinacrine, sulfated polyanions, tetrapyrroles, and modified PrP peptides, [5] have been shown to antagonize prion propagation in cellular and/or animal models of the disease, however their therapeutic use is restricted due to their severe toxicity or their inability to cross the blood-brain barrier. Because tetracycline and iododoxorubicin show structural homology, and as some tetracycline derivatives efficiently cross the blood/brain barrier and have relatively

low toxicity [6, 7] we selected tetracycline for our studies. Indeed, it is known from fluorescence and NMR spectroscopy studies that tetracycline binds to synthetic PrP peptides that are homologous to the sequences spanning residues 82 to 146 (PrP82–146), 106 to 126 (PrP106–126) and 173 to 195 (PrP173–195) [8, 9] of human PrP. Moreover tetracyclines prevent PrP peptide aggregation and the acquisition of protease resistance, disrupt PrP peptide aggregates, and inhibit PrP peptide-induced neuronal death and astroglial proliferation [8, 9]. Furthermore, it has been demonstrated that 20 μM to 2 mM tetracycline concentrations affect the protease resistance of PrP^{Sc} taken from patients with sporadic and new variant CJD, from cattle with bovine spongiform encephalopathy and from 263 K scrapie-infected hamsters [10]. Indeed, those authors used 2 μM tetracycline to induce reversible denaturation of sporadic CJD pathological protein to investigate the effectiveness of tetracycline during drug-protein interaction at the time of PrP^{Sc} folding. Moreover, hamsters injected with an infectious inoculum pre-incubated with tetracycline or doxycycline had a significant delay in the onset of clinical signs and disease progression, and survival time was prolonged [10]. These data suggest that tetracyclines may be regarded as novel anti-prion drugs. The anti-amyloidogenic activity of tetracylines has also been confirmed with other amyloidogenic proteins in *in vitro* and *in vivo* models [11–18]. Finally, a phase II, multicenter, randomized, double-blind, placebo-controlled efficacy study of doxycycline in CJD patients funded by the Italian Agency of Drugs is now in progress.

Tetracyclines are a group of structurally-related antibiotics, presenting five asymmetric centers on a common hydronaphthacene nucleus containing four fused rings (Fig. 1), and their pharmacological and pharmacokinetic properties are well characterized [19–22]. Tetracyclines prevent bacterial growth through different action mechanisms [19]: by binding to the 30S bacterial ribosome and inhibiting protein synthesis, as in the case of doxycycline, minocycline and tetracycline, the most active antibiotic agents; by interacting with bacterial cytoplasmatic membrane, as in the case of anhydrotetracycline. The main features required for antibacterial activity have been well established [20] and, in line with these, clinically used tetracyclines present various substitutions at the 5, 6 and 7 positions.

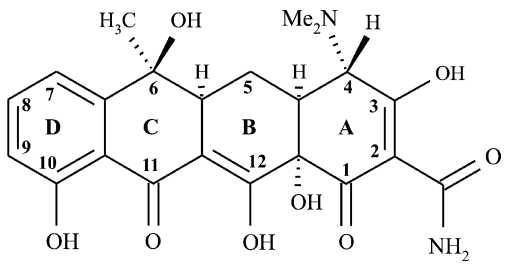

Fig. 1 Chemical structure of tetracycline with atom numbering and ring labels of the hydronaphthacene moiety

Tetracycline solution chemistry is quite complicated due to tetracycline's ability to adopt different protonation states, tautomeric forms and conformations, depending on pH, the presence of metal cations, and the solvent used [23, 24]. The anti-fibrillogenic mechanism of tetracycline derivatives is still unknown, and the influence of pH and metal ions on their activity has not been exhaustively investigated. A better understanding of the stereoelectronic features involved in tetracycline anti-fibrillogenic activity could help define the mechanism of action, and could lead to the design and synthesis of new analogues endowed with enhanced anti-fibrillogenic activity.

Thus, with this as our aim, we carried out anti-fibrillogenic tests on aggregates formed by PrP106–126 with tetracycline and 14 derivatives (TCs), chosen from among commercially available compounds (compounds **1**–**15**, Fig. 2). The paper presents our results and reports the results of a three dimensional quantitative structure activity relationships (3D-QSAR) study carried out to identify the stereoelectronic features affecting the anti-fibrillogenic activity.

3D-QSAR methods are actually faced with thousands of molecular descriptors (variables), and in our investigation we performed a variable reduction step using a recently proposed method [25] called statistical extrema for structure activity model evaluation (SESAME). The search for the best QSAR models was then done using the genetic algorithm - variable subset selection (GA-VSS) method. [26, 27].

Methods

In vitro anti-fibrillogenesis test

Synthetic PrP106–126 was prepared by solid-phase synthesis on a 433A synthesizer (applied biosystems) purified by reverse-phase-HPLC and verified by aminoacid sequencing (46600 Prosequencer, Milligen) and electrospray mass spectrometry (model 5989A, Hewlett-Packard), as previously described [8, 9, 28].

PrP106–126 was dissolved in deionized water at a concentration of 2.0 mM. Aliquots of stock solution were incubated with compounds **1**–**15** at 1:2 peptide:TC molar ratio in 10 mM Tris-HCl, pH 7.0 at a final concentration of 0.5 mM peptide. The samples were kept for 18 hours at 37°C and then subjected to digestion with proteinase K (PK) at 1:100 (w/w) enzyme:substrate ratio. Proteolysis was stopped by adding EGTA (5 mM, final concentration). Following centrifugation, the pellet was dissolved in 10% formic acid containing 0.1% trifluoroacetic acid, and analyzed by reverse

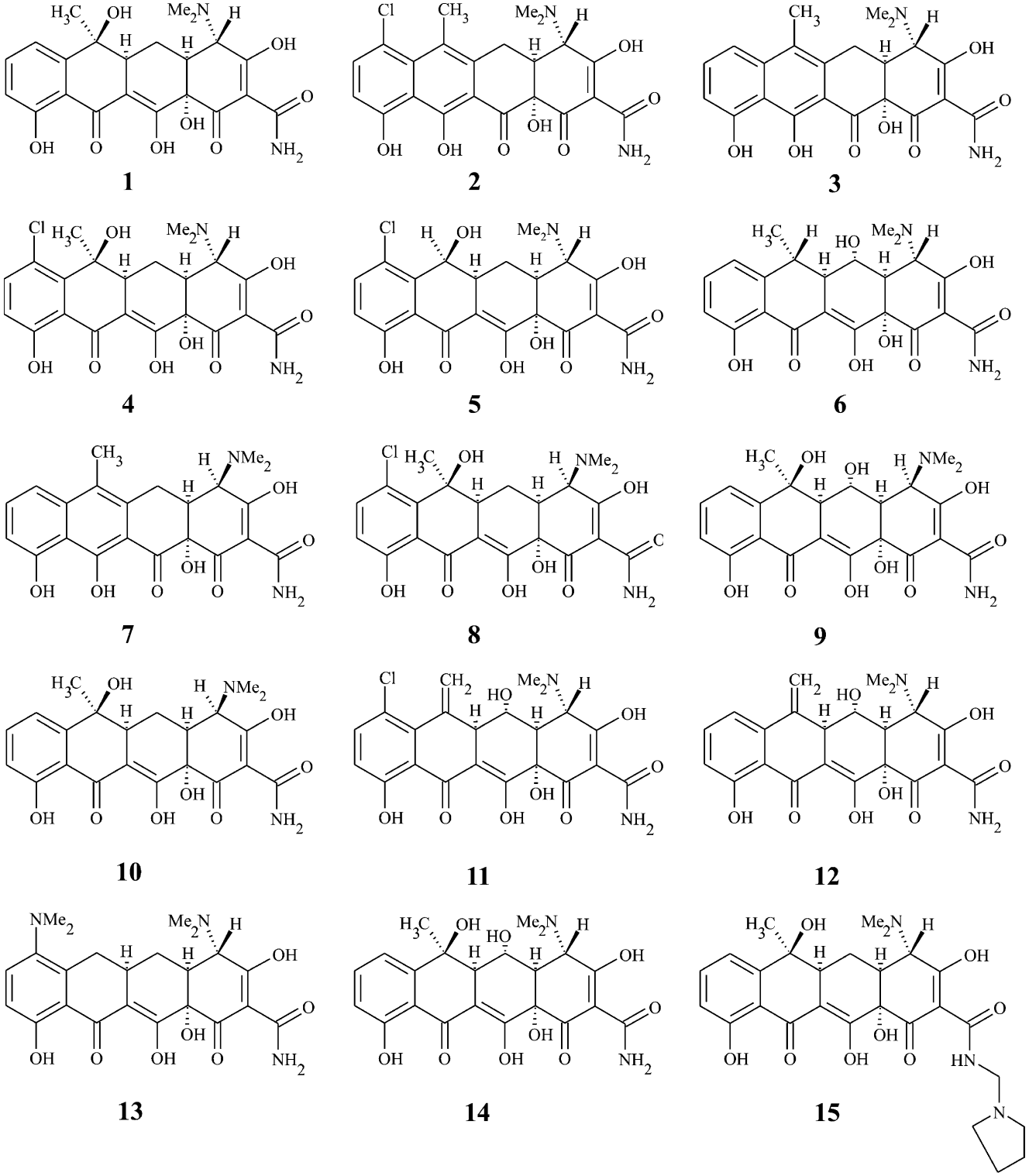

Fig. 2 Chemical structures of the investigated tetracycline analogues: refer to Table 1 for compound names and anti-fibrillogenic activities

phase HPLC. Parallel samples were run in the absence of tetracyclines and analyzed as specified above.

The TC anti-fibrillogenic activity is expressed as the differential activity with respect to the peptide hydrolyzation shown by PK in the absence of TCs. This differential activity is calculated as a percentage, from the difference between the percent of hydrolyzed peptide in the presence ($\%PrP_{TC+PK}$) and absence ($\%PrP_{PK}$) of TCs,

divided by the difference between the total amount of peptide (100%) and $\%PrP_{PK}$:

$$activity = \frac{(\%\,\mathrm{Pr}\,P_{PK+TC}) - (\%\,\mathrm{Pr}\,P_{PK})}{100 - (\%\,\mathrm{Pr}\,P_{PK})} * 100. \quad (1)$$

For each of the compounds **1**–**15**, the activity was determined in two different runs for a total of ten replicates. The average values, together with standard deviations, are shown in Table 1.

3D-QSAR analysis

As biological activities expressed as percentages form a binomial distribution, rather than a normal distribution, the following transformation [29] was applied to the activity values in Table 1:

$$activity' = \arcsin(activity)^{1/2}. \quad (2)$$

Such transformed activity values show a nearly normal distribution, and we used them in the following 3D-QSAR study. Back transformation was achieved by:

$$activity = [\sin(activity')]^2. \quad (3)$$

We had already investigated the conformational space of the considered tetracyclines in aqueous solution by molecular mechanics and *ab initio* methods [30]. In the present 3D-QSAR analysis, all the compounds were considered in the most representative tautomeric form of their neutral protonation state, i.e. the "conventional" zwitterionic form in which the 3-OH group is deprotonated whereas the adjacent 4-NMe_2 group is protonated.

For the lowest energy conformation of each compound calculated by molecular mechanics [30], that is for *extended* conformation, we calculated the partial atomic charges by fitting the molecular electrostatic potential (MEP) computed at the *ab initio* HF-SCF/6–31G** level. The conformations were aligned by rigid-body superimposition of the hydronaphthacene moiety.

The SESAME procedure, performed using software developed in our laboratory, started building an extended 32×29×29 Å, 0.5 Å spaced, 3D grid embedding all the molecules, discarding any grid points lying within the envelope of van der Waals surfaces. At each grid point, the MEP and non-bonded (van der Waals, vdW) interaction energies were calculated for all the molecules, using the above calculated atomic charges and TRIPOS force field parameters (for the methyl probe ε= 0.107 kcal mol^{-1}, and R*=1.70 Å) [31]. For each point we calculated the Pearson correlation coefficient, R, between the biological activities and either the MEP or the vdW values. Then, for each interaction potential, the grid was searched for points presenting local R maximum or minimum values with respect to the first and the second nearest points. To avoid selecting points (descriptors) that are meaningless from the physical or statistical points of view, two additional criteria must be satisfied: i) the standard deviation of the interaction potential values in the point must be greater than a predefined threshold (in our case, 1.0 and 0.05 kcal mol^{-1} for MEP and vdW, respectively), and ii) the absolute value of R in the selected points must be greater than a predefined threshold (in our case R>|0.2|).

Starting from about 200,000 points, SESAME highlighted 40 MEP and 89 vdW descriptors that underwent the GA-VSS technique in the search for regression models with predictive ability. Using software developed in our laboratory we applied the genetic algorithm - variable subset selection (GA-VSS) procedure to search for the best least squares regression models, optimizing the leave-one-out cross validated regression coefficient (Q^2_{LOO}) as an index of the model prediction power.

In order to obtain models that would be interpretable, the search was restricted to models containing four to six independent variables. A population of 100 individuals was generated randomly for each GA-VSS run, and several runs were performed. Finally, for all the possible combinations of training/test set splitting, obtained by including three molecules at a time in the test set (20% cancellation groups), a full cross-validated regression coefficient ($Q^2_{20\%}$) was calculated.

Table 1 Decrease in resistance to proteinase K digestion of PrP106–126 in the presence of **1–15** tetracycline derivatives

Id.	Name	Mean	SD
1	Tetracycline	50.3	3.6
2	Anhydrochlortetracycline	23.4	4.6
3	Anhydrotetracycline	53.7	4.4
4	Chlortetracycline	26.2	2.5
5	Demeclocycline	43.6	6.2
6	Doxycycline	29.6	1.4
7	4-Epianhydrotetracycline	12.4	0.9
8	4-Epichlortetracycline	16.8	1.2
9	4-Epioxytetracycline	52.7	4.7
10	4-Epitetracycline	58.5	5.6
11	Meclocycline	2.7	0.1
12	Methacycline	0.4	0.1
13	Minocycline	0.2	0.1
14	Oxytetracycline	75.7	0.7
15	Rolitetracycline	77.9	11.7

[(a)] In the experimental conditions: $(\%PrP_{PK})$=50.0±2.5
Differential activities (%) with respect to that of PK alone are calculated by Eq. (1).[(a)] Average values (± SD) from ten replications in two different experiments.

Results and discussion

PrP106–126 consists of an N-terminal polar head (KTNMKHM) followed by a long hydrophobic tail (AGAAAAGAVVGGLG); it tends to form a β-sheet secondary structure, has a strong tendency to aggregate into fibrils, and shows partial resistance to protease digestion. These properties are similar to those of the full-length PrP, suggesting that PrP106–126 may represent a segment of PrP that is involved in the conformational transition from PrP^{C} to PrP^{Sc} [2]. For these reasons the PrP106–126 peptide is a widely used model system for the *in vitro* investigation of the pathological PrP protein.

Table 1 shows the differential anti-fibrillogenic activity of the **1**–**15** tetracycline derivatives tested on PrP106–126 peptide. The results of the anti-fibrillogenesis test show that there were marked differences in the anti-fibrillogenic activity of the 15 congeners, indicating that the changes in the substitution pattern of the hydronaphthacene nucleus play a critical role in the proteolysis activity. Worthy of note is the fact that Oxytetracycline (**14**) and Rolitetracycline (**15**) were significantly more active than the other molecules.

All the tetracylines considered in this paper have antibacterial activity, thus all of them present the main required structural features [20]. Indeed, the lower "hydrophilic" part, which is involved in the structural requirements for antibiotic activity, is very similar in structure in all the compounds. Thus the structural variability of this data set lies in the "hydrophobic" part of the molecules: substitution at the 5, 6 and 7 positions; stereochemical configurations at the 4 position, labeled in the following as *epi* (compounds **7**–**10**) and *non-epi*; the aromatization of the C-ring with the consequent switch of the keto-enolic system between positions 11 and 12 (compounds **2**, **3**, and **7**).

We had already carried out a preliminary investigation [30] into the possibility of relationships between the conformational flexibility of the hydronaphthacene moiety and the anti-fibrillogenic activity. Two main conformational families were detected for TCs, an *extended* (energetically favored) conformation and a *folded* one that differ in the A-ring spatial arrangement. However, despite the conformational flexibility of the considered tetracyclines, we were unable to identify a geometrical pharmacophore that justified the differences observed in the activity. These negative results prompted us to analyze, through 3D-QSAR analysis, the stereoelectronic properties of this class of compounds in their *extended* conformation: for a set of properly aligned molecules, the interaction energy is calculated using one or more probes in a 3D grid of points embedding the molecules; the resulting values are then used as descriptors for the QSAR search. The search for the best QSAR models is generally performed by genetic algorithms [26, 27] rather than by the partial least squares method [32] as in CoMFA [33]. Apart from the molecular alignment problem, the 3D-QSAR approach is faced with having to consider thousands of molecular descriptors. This has led to the proposal of several different strategies suitable for selecting only those descriptors likely to yield regression models with predictive ability [34, 35].

In the present analysis we used the SESAME variable reduction technique. This was tested on the steroid benchmark and provided models that not only compare well with those obtained by the CoMFA method, but that also show higher predictive ability [25].

The SESAME technique identifies, from among the grid points, the local maximum (or minimum) values of a suitable statistical index, such as the Pearson correlation coefficient (R) calculated between biological activity and interaction potential distributions. The considered interaction potentials were the MEP and the vdW interaction potentials. The SESAME technique relies on continuous variation in the molecular interaction potentials: points with local maximum (or minimum) R values best summarize the information of the surrounding regions with regard to potential distribution and activity correlation, and are thus the best descriptor candidates for QSAR analysis. Having selected the best descriptor candidates for QSAR analysis, the search for the best models begins and is performed using the GA-VSS method.

As our data set was quite small in size, no external test set was considered for the model validation step, instead all 15 compounds were used in a full cross-validation procedure (with 20% cancellation groups) to assess the

Table 2 Best set of models obtained by the regression procedure

R^2	R^2_{adj}	Q^2_{LOO}	$Q^2_{20\%}$	Standard error	F	Standardized regression coefficients					
						$V_{vdW}1$	$V_{MEP}2$	$V_{MEP}3$	$V_{vdW}4$	$V_{MEP}5$	$V_{vdW}6$
0.991	0.984	0.971	0.964	2.42	142.3	0.774 (.035)	−0.335 (.038)	0.266 (.057)	−0.243 (.041)	−0.134 (.054)	0.092 (.037)
0.983	0.974	0.958	0.950	3.06	106.5	0.783 (.044)	−0.316 (.047)	0.313 (.068)	−0.268 (.051)	−0.108 (.066)	
0.979	0.970	0.947	0.943	3.30	113.7	0.786 (.047)	−0.312 (.050)	0.395 (.049)	−0.302 (.050)		

Reported for each model are: the fitting (R^2) and the adjusted (R^2_{adj}) correlation coefficients; the leave-one-out cross validated regression coefficient (Q^2_{LOO}); the full cross-validated regression coefficient with 20% cancellation groups ($Q^2_{20\%}$); the standard error and the F value; the standardized regression coefficients (with standard errors in brackets) of each variable entering the models.

predictive ability of the best models found by GA-VSS. In this procedure, the activity of three of the data set molecules was calculated by the model built from the other 12 compounds; this procedure was repeated for every possible triplet of molecules (for a total of 455 triplets); the average cross-validated regression coefficient, $Q^2_{20\%}$, was then calculated. Thus $Q^2_{20\%}$ represents a tight test for the prediction ability of the models.

The population of best models obtained by GA-VSS was then analyzed to identify models with high predictive power, physical meaning, and stability to the increase in numbers of variables entering the models. One set of models had the desired properties and is summarized in Table 2. The values of the molecular descriptors in the model set, i.e. the MEP and vdW interaction potential values in the grid points, are reported in Table 3 alongside the Pearson correlation coefficient values (R). Table 4 shows the activity values calculated by the 4- to 6-variable models, together with the experimental values.

The model set exhibits good statistical quality, both in fitting (R^2 0.979–0.991) and in prediction (Q^2_{LOO} 0.947–0.971; $Q^2_{20\%}$ 0.943–0.964). Furthermore, on increasing the number of variables the model not only remains stable but also improves in quality. In fact, the descriptors present in the 4-variable model are also included in the 5- and 6-variable models, and those in the 5- are present in the 6-variable model. Moreover, these models have a physical grounding as the role played by the model descriptors can be interpreted on the basis of chemical structure. The spatial disposition of the descriptors entering the 3D-QSAR model around the aligned tetracycline structures is shown in Fig. 3. Although the experimental anti-fibrillogenic activity depends on all the descriptors entering the model, also the individual contribution of the single variables taken one at a time can provide useful information; this leads to the following remarks.

Table 3 Values of the descriptors (MEP and vdW interaction potentials, kcal mol^{-1}) within the best set of models, together with the Pearson correlation coefficient values (R) calculated between the biological activity and the interaction potential values

	R	$V_{vdW}1$	$V_{MEP}2$	$V_{MEP}3$	$V_{vdW}4$	$V_{MEP}5$	$V_{vdW}6$
		0.759	−0.372	0.369	−0.396	−0.457	0.246
Mol. Id.							
1		−0.269	−21.54	−14.1	−0.459	44.90	−0.315
2		−0.373	−11.27	−15.4	−0.861	43.09	−0.255
3		−0.364	−27.42	−15.8	−0.854	42.66	−0.255
4		−0.338	−8.45	−14.9	−0.462	45.73	−0.003
5		−0.222	−3.41	−12.7	−0.163	43.44	−0.303
6		−0.480	−25.14	−6.4	−0.532	37.81	−0.301
7		−0.402	−24.31	−16.3	−0.408	48.07	−0.354
8		−0.331	−9.88	−15.1	−0.303	42.63	−0.319
9		−0.344	−23.96	−8.6	−0.238	41.01	−0.109
10		−0.285	−23.01	−13.3	−0.413	43.15	−0.393
11		−0.437	−3.98	−12.2	−0.435	42.76	−0.324
12		−0.483	−16.50	−13.5	−0.220	45.48	−0.305
13		−0.486	−16.58	−10.1	−0.056	42.49	−0.300
14		−0.285	−19.57	−9.7	−0.587	37.52	−0.248
15		−0.309	−19.47	−1.4	−0.475	40.45	−0.185

Table 4 Experimental activities and calculated values by the 4- to 6-variable models

Id.	Name	Exp.	Calc.[a]		
			4-var	5-var	6-var
1	Tetracycline	50.3	57.8	58.0	56.6
2	Anhydrochlortetracycline	23.4	27.6	27.6	27.1
3	Anhydrotetracycline	53.7	55.7	50.3	51.4
4	Chlortetracycline	26.2	16.4	18.5	24.4
5	Demeclocycline	43.6	43.4	42.3	40.6
6	Doxycycline	29.6	28.5	28.8	28.0
7	4-Epianhydrotetracycline	12.4	12.0	13.0	11.8
8	4-Epichlortetracycline	16.8	27.0	19.6	19.1
9	4-Epioxytetracycline	52.7	48.4	48.0	53.2
10	4-Epitetracycline	58.5	61.1	57.5	54.3
11	Meclocycline	2.7	2.2	2.9	2.1
12	Methacycline	0.4	0.2	0.2	0.1
13	Minocycline	0.2	1.2	0.8	0.9
14	Oxytetracycline	75.7	80.2	75.1	75.5
15	Rolitetracycline	77.9	60.5	79.3	78.5

[a] Reported values are back transformed from (*activity'*): see Methods section.

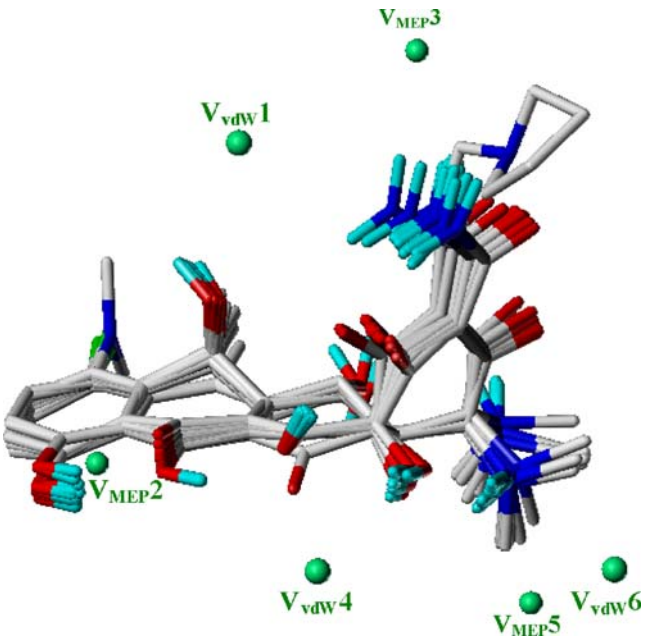

Fig. 3 Spatial disposition around the aligned structures of the considered tetracyclines of the descriptors within the best set of 3D-QSAR models: refer to Table 3 for descriptor and Pearson correlation coefficient values at each point

The $V_{vdW}1$ variable, which presents the highest standardized coefficient in all the models (Table 2), lies above the C-ring and is related to the presence/absence of the 6-OH group. As the standardized coefficient of the $V_{vdW}1$ variable is positive, less negative vdW potential values will increase the predicted activity. Thus, as the less negative vdW interaction potential values (Table 3) belong to compounds containing the 6-OH group, enhanced activity will only be achieved if this group is present.

The $V_{MEP}2$ variable, the second most important variable in all the models, is located below the center of the D aromatic ring. Due to the π-electron distribution, all the molecules have negative MEP values in this region. Indeed, the variable standardized coefficient is negative, and the more negative the MEP values the greater the activity. Chlorine substitution at position 7 (compounds **2**, **4**, **5**, **8**, and **11**) decreases the electron density on the aromatic ring; this makes the molecular electrostatic potential less negative and leads to decreased activity. Aromatization of the C-ring (compounds **2**, **3** and **7**) enriches the π-electron system in the D-ring slightly, resulting in more negative MEP values and, potentially, in greater activity.

The $V_{MEP}3$ variable has a positive regression coefficient and the MEP values for compounds **15**, **6**, **9**, and **14** are less negative. Of these compounds, compound **15** has the least negative MEP, an effect driven by the presence of the pyrrolidinic substituent at the amidic group in position 2. Instead, in compounds **6**, **9**, and **14** it is the 5-OH group that influences the MEP values, though such influence is only slight. As a secondary effect, the most negative MEP is in the anhydrous compounds, due to the presence of the ketonic group in position 12. Thus the model suggests that the presence of an alkylamine substituent at the amidic group in position 2 and the 5-OH group (making MEP less negative) should enhance activity, while the switching of the keto-enolic system should reduce it.

The $V_{vdW}4$ variable has a negative regression coefficient, and its values are tuned by both the stereochemical configuration at position 4 and the spatial disposition of 6-Me. The *epi* configuration renders the potential less negative, while an appropriate spatial disposition of 6-Me (compounds **2** and **3**) results in more negative vdW values. The effect of a *non-epi* configuration on activity is also due to the $V_{vdW}6$ variable.

Finally, the $V_{MEP}5$ variable has a negative coefficient and shows positive and large MEP values for all the compounds due to the proximity of the positively charged NMe_2 group: the presence of a hydroxyl group at position 5 renders the MEP values less positive (compare, for instance, compounds **1** and **14**, or **10** and **9**), thus increasing the activity. As a consequence, it can be expected that the inclusion of a 5-OH substituent will further increase the activity of compound **15**.

Summary

The 3D-QSAR investigation has highlighted that hydroxyl groups at positions 5 and 6 are important factors in determining anti-fibrillogenic activity, providing donor sites for putative H-bond interactions with peptides. A second relevant factor is that the presence of electrodonor substituents on the D-ring enhances the π-electron density of the aromatic ring: this effect can set up favorable π-stacking interactions with electron deficient peptide sites. Also an alkylamine substituent at the amidic group in position 2 favors activity, providing another site for interaction with the peptides. Moreover, the *non-epi* configuration contributes to activity, ensuring the correct spatial orientation of the positively charged NMe_2 group in electrostatic interactions with negatively charged sites. On the contrary, switching the keto-enolic system between positions 11 and 12 decreases the activity, even though an aromatic C-ring could act as an electrodonor substituent at the D-ring.

This model, factorizing the contributions of the different functional groups, provides the basis for the rationalization of the observed anti-fibrillogenic activity, including that of the most active oxytetracycline **14** and rolitetracycline **15** compounds. To verify the influence of the conformational flexibility of the hydronaphthacene moiety on the relative spatial disposition of the functional groups, further investigations will be carried out starting from the *folded* conformation.

In conclusion, our 3D-QSAR model unveils the main stereoelectronic features affecting the anti-fibrillogenic activity of this class of compounds. Thus, advantage can now be taken of this acquired knowledge, and we can use the information to design, synthesize and test novel tetracycline congeners endowed with enhanced anti-fibrillogenic activity.

Acknowledgements We gratefully acknowledge financial supports from the Italian Ministry of University and Research (PRIN 2001, PRIN 2003, FIRB Protocol RBNE03PX83) the European Union (Neuroprion and Heteroprion networks, Contract FOOD-CT-2004-506579), the Negri-Weizmann Foundation, and the Fondazione Cariplo (Grant NOBEL-GUARD).

References

1. Prusiner SB (1998) Proc Natl Acad Sci USA 95:13363–13383
2. Tagliavini F, Forloni G, D'Ursi P, Bugiani O, Salmona M (2001) Studies on Peptide Fragments of Prion Proteins. In: Caughey B (ed) Advances in Protein Chemistry - Volume 57. Academic, San Diego, pp 171–202
3. Bessen RA, Kocisko DA, Raymond GJ, Nandan S, Lansbury Jr PT, Caughey B (1995) Nature 375:698–700

4. Kocisko DA, Come JH, Priola SA, Chesebro B, Raymond GJ, Lansbury PT, Caughey B (1994) Nature 370:471–474
5. Forloni G, Varì MR, Colombo L, Bugiani O, Tagliavini F, Salmona M (2003) Curr Med Chem - Immun Endoc Metab Agents 3:185–197
6. Sande MA, Mandell GL (1990) Antimicrobial Agents. In: Gilman AG, Rall TW, Nies AS, Taylor P (eds) The Pharmacological Basis of Therapeutics, 8th edn. Pergamon, New York, pp 1085–1092
7. Howlett DR, George AR, Owen DE, Ward RV, Markwell RE (1999) Biochem J 343:419–423
8. Tagliavini F, Forloni G, Colombo L, Rossi G, Girola L, Canciani B, Angeretti N, Giampaolo L, Peressini E, Awan T, De Gioia L, Ragg E, Bugiani O, Salmona M (2000) J Mol Biol 300:1309–1322
9. Ronga L, Langella E, Palladino P, Marasco D, Tizzano B, Saviano M, Pedone C, Improta R, Ruvo M (2007) Proteins: Structure, Function, and Bioinformatics 66:707–715
10. Forloni G, Iussich S, Awan T, Colombo L, Angeretti N, Girala L, Bertani I, Poli G, Caramelli M, Grazia Buzzone M, Farina L, Limido L, Rossi G, Giaccone G, Ironside JW, Bugiani O, Salmona M, Tagliavini F (2002) Proc Natl Acad Sci USA 99:10849–10854
11. Chen M, Ona VO, Ferrante RY, Fink KB, Zhu S, Bian J, Guo L, Farrell LA, Hersch SM, Hobbs W, Vousattel JP, Cha JH, Friedlander RM (2000) Nat Med 6:797–801
12. Du Y, Ma Z, Lin S, Dodel RC, Gaom F, Bales KR, Triarhou LC, Chernet E, Perry KW, Nelson DL, Luecke S, Phebus LA, Bymaster FP, Paul SM (2001) Proc Natl Acad Sci USA 98:4669–14674
13. Forloni G, Colombo L, Girala L, Tagliavini F, Salmona M (2001) FEBS Lett 487:404–407
14. Aitken JF, Loomes KM, Kornarkowska B, Cooper GJS (2003) Biochem J 374:779–784
15. Cardoso I, Merlini G, Saraiva MJ (2003) FASEB J 17:803–809
16. Smith DL, Woodman B, Mahal A, Sathasivam K, Ghazi-Noori S, Lowden PAS, Bates GP, Hockly E (2003) Ann Neurol 54: 186–196
17. Malmo C, Vilasi S, Iannuzzi C, Tacchi S, Cametti C, Irace G, Sirangelo I (2006) FASEB J 580:346–367
18. Ono K, Yamada M (2006) J Neurochem 97:105–115
19. Chopra I (1994) Antimicrob Agents Chemother 38:637–640
20. Chopra I, Roberts M (2001) Microbiol Mol Biol Rev 65:232–260
21. Mitscher LA (1978) Medicinal Research Series Vol. 9: The Chemistry of Tetracycline Antibiotics. Dekker, New York
22. De Leenheer AL, Nelis HJ (1979) J Pharm Sci 68:999−1002
23. Schneider S (2001) Proton and Metal Ion Binding of Tetracyclines. In: Greenwald RA, Hillen W, Nelson M (eds) Tetracyclines in Biology Chemistry and Medicine. Birkhaüser Verlag, Basel, p 65−104
24. Othersen OG, Beierlein F, Lanig H, Clark T (2003) J Phys Chem B 107:13743−13749
25. Cosentino U, Moro G, Bonalumi D, Bonati L, Lasagni M, Todeschini R, Pitea D (2000) Chemometr Intell Lab Syst 52: 183−194
26. Leardi R, Boggia R, Terrile M (1992) J Chemom 6:267−281
27. Goldberg DE (1989) Genetic Algorithms in Search Optimization and Machine Learning. Addison-Wesley, Boston
28. De Gioia L, Selvaggini C, Ghibaudi E, Diomede L, Bugiani O, Forloni G, Tagliavini F, Salmona M (1994) J Biol Chem 269:7859–7862
29. Zar JH (1984) Biostatistical Analysis. Prentice-Hall, Englewood Cliffs, NJ
30. Cosentino U, Varì MR, Saracino AAG, Pitea D, Moro G, Salmona M (2005) J Mol Mod 11:17–25
31. Clark M, Cramer RD III, Van Opdenbosch N (1989) J Comp Chem 10:982–1012
32. Wold S, Sjostrom M, Eriksson L (2001) Chemometr Intell Lab Syst 58:109–130
33. Cramer RD, Patterson DE, Bunce JD (1988) J Am Chem Soc 110:5959–5967
34. Baroni M, Costantino G, Cruciani G, Riganelli D, Valigi R, Clementi S (1993) Quant Struct-Act Relat 12:9–20
35. Lindgren F, Geladi P, Rännar S, Wold S (1994) J Chemom 8:349–363